CFD VALIDATION OF INCOMPRESSIBLE CROSS-FLOW DISCHARGE COEFFICIENTS

Q. G. Rayer

Rolls-Royce Plc, P.O. Box 31, Derby, DE24 9DH

1. SUMMARY

Validation against air systems problems is required to enable Computational Fluid Dynamics (CFD) codes to be confidently used in the design of turbine cooling air systems. CFD calculations of orifice cross-flow discharge coefficients (C_d) have been compared with measurements by Rohde et al [1]. Simulations have been carried out for cases with a low main duct Mach number ($M_d \leq 0.25$) using incompressible flow modelling. Comparisons have been made of cross-flow discharge coefficients for a range of pressure-head ratios and Mach numbers. Results at a main duct Mach number of 0.07 were obtained using the standard k-ε turbulence model which gave agreement to better than 5% for absolute values of pressure-head ratios and discharge coefficients. The trends in the data for pressure-head ratios and Mach numbers were also reproduced. At a higher main duct Mach number of 0.25, the Mach number in the vicinity of the orifice reached 0.8. As expected this rendered incompressible flow modelling unsuitable, resulting in inaccurate determinations of orifice pressure-drops. Work is already in progress to simulate high Mach number cases using a more suitable compressible flow model. The results obtained so far give confidence that CFD will become a valuable tool for evaluating air system losses in novel configurations.

1.1 Symbols and Notation

The symbols and notation have generally been chosen to follow Rohde et al [1].

A_d Area of main duct, m^2.

A_o Area of orifice, m^2.

C_d Orifice cross-flow discharge coefficient.

C_P Specific heat capacity for air, $J.kg^{-1}.K^{-1}$.

d Orifice diameter, m.

M_d Mach number of flow in main duct.

PHR Pressure head ratio, $PHR = \left(P_T - p_j\right) / \left(P_T - p_d\right)$.

P_T Total pressure in main duct, Pa.

p_d Static pressure in main duct, Pa.

p_j Static pressure in orifice jet, Pa.

R Gas constant for air, 287.012 $J.kg^{-1}.K^{-1}$.

T_d Main duct static temperature, K.

T_T Main duct total temperature, K.

t Orifice thickness, m.

V_d Main duct air velocity, $m.s^{-1}$.

V_j Orifice jet air velocity, $m.s^{-1}$.

w_d Mass flow rate out of main duct, $kg.s^{-1}$.

w_o Mass flow rate through orifice, $kg.s^{-1}$.

γ Ratio of specific heats for air, $=(1-R/C_p)^{-1}=1.399$.

ρ_d Main duct air density, $kg.m^{-3}$.

ρ_j Orifice jet air density, $kg.m^{-3}$.

1.2 Motivation

Gas turbine internal cooling air systems perform several functions of which the most important are turbine blade/vane cooling, ventilation of rotating components and the sealing of turbine cavities against hot core flow gas ingress. These functions are critically important in ensuring the integrity of highly stressed rotating components. A significant proportion of the total core mass flow is used in the internal air system with a consequent increase in turbine entry temperature at take-off conditions, and of specific fuel

consumption at cruise. In order to minimise running costs, it is essential that the flow delivered by the system matches the requirement as closely as possible.

Traditional methods of analysing gas turbine internal air systems have been to use one-dimensional network simulations. The representation of complex loss features has been by correlations representing empirical sources of data. These include standard sources from the published literature such as Rohde et al [1], and for features particular to gas turbines, specially commissioned research data. This is unsatisfactory for two reasons:

- Practical considerations mean that it is often inconvenient to design loss features in the same way as the ideal geometries tested by researchers.
- The market is extremely competitive, making it undesirable to support extensive research activity unless there is no alternative.

It is clearly very important to develop new methods of deriving losses, which allow better use to be made of research data and allow novel components to be investigated.

Computational fluid dynamics flow simulations offer the prospect of rapid and accurate simulation of air-systems problems. To give confidence that CFD calculations will prove sufficiently accurate for use within Rolls-Royce, and to establish guidelines for CFD code use, it is necessary to undertake a programme of code validation against relevant air-systems problems. While fairly low solution accuracies (say 20% or so) may be adequate for certain classes of air systems problems (e.g. determination of the relative merits of different configurations or flow visualisation studies), other applications would require a proven accuracy to at least 10% and preferably better than 5% for static pressures, pressure-differences, velocities and temperatures.

CFD calculations are carried out for complex geometries within Rolls-Royce to determine the relative merits of different gas turbine component configurations. In addition the critical significance of establishing the absolute quantitative accuracy of simulations has not been neglected. As a step in a CFD validation programme against the absolute values of flow parameters for a range of geometries, the simplest possible relevant systems have been chosen for which quantitative data is available, before moving on to more complex

geometries. This commenced with air flow through an orifice [2, 3] and has progressed to cross-flow orifice discharge coefficients, the subject of the present paper. The results and methodology assist in the generation of a database of configurations solved to a known accuracy as well as the generation of guidelines for best practice in CFD [4]. As the programme continues the experience gained will contribute to accurate validation against flows in more complex geometries including rotor-stator systems and other configurations relevant to gas turbine applications, and for which Rolls-Royce has access to high-quality quantitative data. The experience gained, even for the simple orifice geometry [2, 3], has shown that achieving absolute accuracies of (say) 5% is not as straightforward as might be expected. This is consistent with the experience of Hay and Lampard [5] for the more complex problem of modelling a hole in a rotating disc, where although relative C_d calculations gave good agreement, absolute values were about 15% lower than measurements.

2. SPECIFICATION OF PROBLEM

The current report covers the case of cross-flow for a circular outlet orifice in the side-wall of a duct. The inlet air flow enters a straight duct of circular cross-section. At some point along the duct a small side-orifice draws a proportion of the flow from the main duct, while the remainder of the flow exits from the main duct outlet. The geometry is illustrated in Figure 2.1. Data for validation was obtained from Rohde et al [1].

The geometry consisted of a circular main duct of radius 3.15mm and length 90mm. A circular orifice mid-way along the duct pierced the side-wall. The orifice had a radius $(d/2)$ of 1.622mm and a thickness (t) of 1.65mm and discharged into a circular collection duct of radius 3.15mm and length 40.2mm. The centre-lines of both the orifice and the orifice collection duct were coincident and met the centre-line of the main duct at a right-angle.

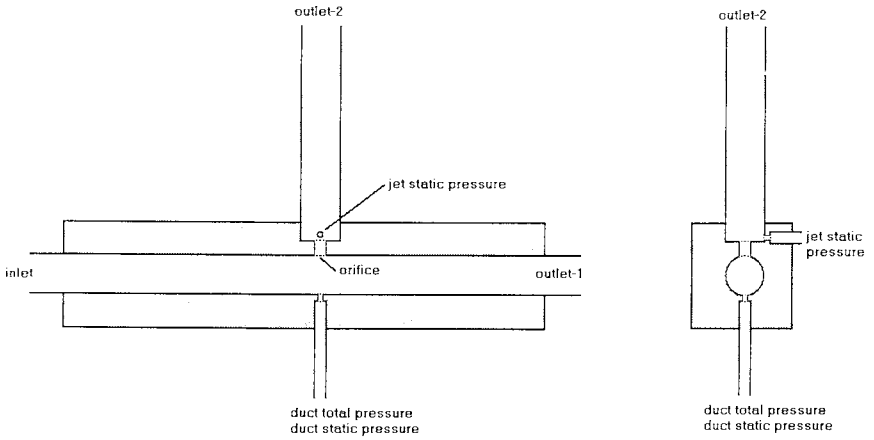

Figure 2.1: Cross-flow geometry.

2.1 Purpose of Analysis

The current report details the results of simulation of one of a class of flows involving ducts with side-wall apertures at low Mach numbers so that incompressible flow models can be used. The range of conditions covered are based on Rohde et al [1] and have been compared with some typical engine conditions in Figure 2.2.

Incompressible flow modelling allows a more rapid model convergence than would be possible with the available computing capability for compressible flow simulations. This permits a greater range of conditions to be covered than otherwise, although placing a restriction on the maximum permissible M_d that can be used (here $M_d \leq 0.25$). A further validation exercise will be carried out to cover compressible simulations of cases at higher M_d also presented in [1]. Completion of these 'cross-flow' studies prepares the way for validation of more realistic systems such as flow through a hole in a rotating disc.

Hay and Lampard's simulations gave C_d 15% lower than measured values [5], which are outside the 5% accuracy requirements for air systems.

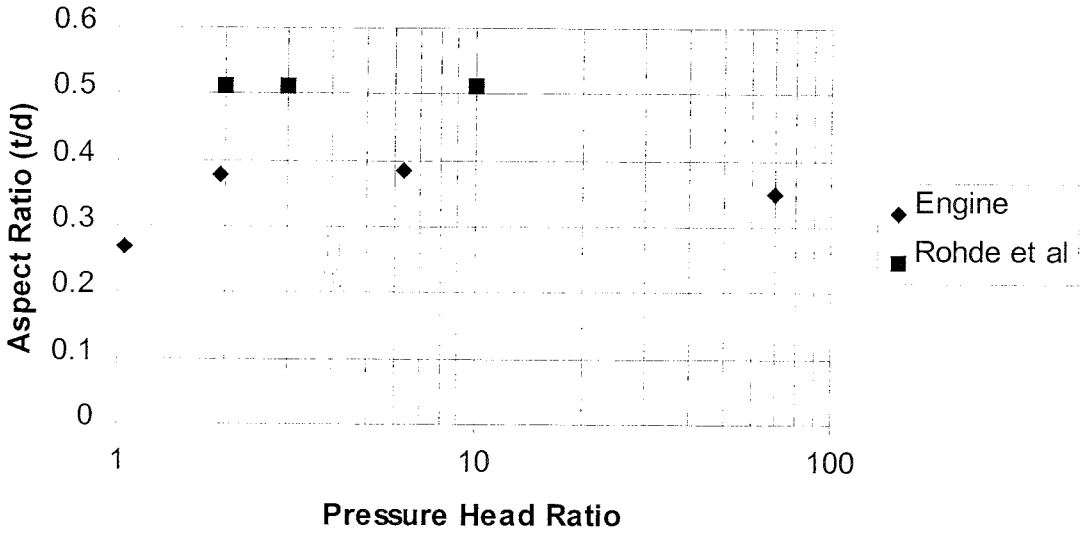

Figure 2.2: Comparison between cross-flow data [1] and engine conditions. Points for engine conditions derived for Trent 8104, R010, R251, R290 and R410 holes.

2.2 Special Features

The experimental data collected by Rohde et al [1] were correlated and presented in terms of curves for given duct air-flow Mach numbers. Although Mach numbers in the range 0.01 to ~0.65 were covered, in the present work only data relating to flows with Mach numbers of 0.25 or less were considered, so that incompressible flow modelling could be used. The form of the correlation involved plotting a C_d against a pressure-difference ratio (pressure-head ratio, PHR). The methods used to define the C_d and the PHR are covered in section 3.

3. RELATED EXPERIMENTS AND ANALYTICAL SOLUTIONS

The Rohde et al [1] data for comparison with the CFD simulations consisted of a means of defining C_d, and correlation against PHR for a given M_d.

3.1 Global Parameters

Following [1], the orifice C_d is defined as the ratio of the actual flow to the ideal flow,

$$C_d = \frac{w_o}{\rho_j . V_j . A_o}. \qquad (1)$$

The values of the ideal jet velocity and density were determined from the equations for compressible flow

$$V_j = \sqrt{\frac{2\gamma R T_T}{(\gamma - 1)} . \left[1 - \left(\frac{p_j}{P_T} \right)^{\frac{\gamma - 1}{\gamma}} \right]}, \qquad (2)$$

and

$$\rho_j = \frac{p_j}{R T_T} . \left(\frac{P_T}{p_j} \right)^{\frac{\gamma - 1}{\gamma}} \qquad (3)$$

Note that these equations limit the jet velocity to the speed of sound [1], because the orifice does not contain a divergent section to permit supersonic flow. In the current case this is of no concern as the modelling limitations of incompressible flow would limit the CFD simulations to a maximum Mach number of around 0.3. In fact a maximum duct M_d of 0.25 was used.

In equation (2) the main duct total pressure, P_T was used to estimate the total pressure in the jet. While the main duct static pressure would give a more suitable reference pressure for the case when the approach flow is perpendicular to the orifice axis (so there is no velocity head pressure recovery), Rohde et al [1] point out that the main duct total pressure can also be used when the orifice is inclined to the main duct axis, in which case some of the velocity head is recovered.

The main duct total pressure was determined by an iterative procedure using the following equations.

$$P_T = p_d . \left[1 + \left(\frac{\gamma - 1}{2} \right) M_d^2 \right]^{\frac{\gamma}{\gamma - 1}}, \qquad (4)$$

$$M_d = \frac{V_d}{\sqrt{\gamma R T_d}}, \qquad (5)$$

$$V_d = \frac{w_d}{A_d \cdot \rho_d}, \qquad (6)$$

$$\rho_d = \frac{p_d}{R T_d}, \qquad (7)$$

$$T_d = \frac{T_T}{\left[1 + \left(\frac{\gamma - 1}{2}\right) M_d^2\right]} \qquad (8)$$

The definitions of the symbols used are given at the front of the current paper.

Also define the pressure-head ratio (pressure-difference ratio), PHR as

$$PHR = \frac{P_T - p_j}{P_T - p_d}. \qquad (9)$$

3.2 Presentation of Data by Rohde et al.

The data from [1] defines C_d as a function of M_d and PHR, for a given geometry. Thus each data point essentially consists of a C_d, M_d and PHR for a rig configuration. The data points selected for the current (incompressible) validation are presented in Table 3.1, with the other data required in Table 3.2.

Geometry	Target Discharge Coefficient, C_d	Target Pressure-Head Ratio, PHR	Mach Number, M_d
Model 1	0.4	3.0	0.07
Model 1	0.3	2.0	0.07
Model 1	0.58	10.0	0.07
Model 1	0.65	10.0	0.25

Table 3.1: Target Data points from [1]. Rohde et al used a range of geometries denoted as different models. 'Model 1' refers to the geometry with $t/d = 0.51$, the only geometry considered in the present paper.

Pressure Head Ratio, PHR	C_d at $M_d = 0.07$	C_d at $M_d = 0.25$
1.0	0.000	0.000
1.5	0.200	0.200
2.0	0.300	0.300
3.0	0.400	0.423
4.0	0.472	0.500
5.0	0.512	0.546
6.0	0.535	0.581
8.0	0.569	0.624
10.0	0.588	0.656
15.0	0.612	-

Table 3.2: Data used for comparison in the validation [1]. Discharge coefficients at intermediate values of PHR were obtained by linear interpolation.

In effect Rohde et al [1] present results for $C_d = f_{\text{expt}}(M_d, PHR)$, where the functional form of f_{expt} is provided in graphical form. By selecting values of C_d, M_d and PHR from Rohde et al the current validation seeks to check that in the equivalent formulation for the CFD simulation $C_d = f_{\text{cfd}}(M_d, PHR)$, it can be demonstrated that f_{cfd}=f_{expt} to an acceptable accuracy.

3.3 Definition of y^+

In the CFD modelling the wall units $y^* \equiv \rho C_\mu^{1/4} k_P^{1/2} y_P . \mu^{-1}$ and $y^+ \equiv \rho u_\tau y_P . \mu^{-1}$ are used in the wall function correlation representing the Reynolds boundary layers, following FLUENT [6]. The wall functions are defined in terms of y^*, however both y^* and y^+ have comparable values when the first cell adjacent to the wall is placed in the wall log-layer. The wall function correlation can generally be used for y^+ values in the range 20-300. For further details see the FLUENT user's guide [6] or Versteeg and Malalasekera [7].

4. SPECIFICATION OF CFD MODEL

4.1 Overall Validation Strategy

In order to give confidence that CFD can reproduce cross-flow effects, it is important that validation should extend beyond a single case, so that apart from a quantitative 'spot-check', the ability of FLUENT to predict the trend in the experimental data is also validated. Rohde et al [1] give C_d as a function of PHR and M_d, thus the quantitative dependencies on both of these variables must be simulated. As incompressible flow has been assumed in the current work, the maximum M_d tried was 0.25.

In addition to the above a mesh sensitivity study was required. The cases covered are summarised in Figure 4.1.

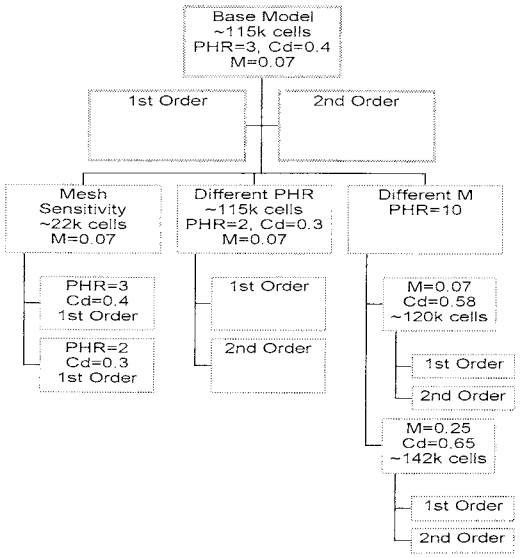

Figure 4.1: Diagram showing range of validation cases covered, shown as sensitivity studies relative to a 'base model'.

4.2 Model Set-up and Analysis of Results

The equations in section 3.1 used to define C_d do not readily lend themselves to the analysis of any CFD flow solution obtained. A further difficulty is that while it is perfectly feasible in a laboratory to adjust an outlet valve until some appropriate pressure reading meets the desired value, this approach is grossly impractical for CFD validation. Thus a method was developed to allow the FLUENT simulation to be set up with boundary conditions that would select a specific data point, with a similar approach used to analyse the results of a converged CFD solution.

4.2.1 Model Set-up

A set of values for C_d, PHR and main duct M_d was selected from the data presented in [1]. These were used to derive the ratio of mass flow rates between the main duct outlet and the orifice outlet (such a mass flow split is straightforward to define as a model boundary condition in FLUENT) as follows.

The duct static temperature was assumed fixed at a value $T_d = 303K$. Rohde et al [1] state that the main duct static pressure was held at a nominal value of $p_d = 2.76 \times 10^5 Pa$, so this value was also assumed. The geometry means that the areas of the duct, A_d and orifice, A_o are also defined, so that equation (7) can be solved. In addition equation (8) can be re-arranged to give,

$$T_T = T_d\left[1+\left(\frac{\gamma-1}{2}\right)M_d^2\right], \qquad (10)$$

and re-arrangement of (5) yields,

$$V_d = M_d \cdot \sqrt{\gamma R T_d}\,. \qquad (11)$$

Now the main duct exit mass flow rate can be calculated from (6)

$$w_d = V_d \,.\, A_d \,.\, \rho_d\,. \qquad (12)$$

Next the main duct total pressure can be determined using (4). As the PHR for the data point under consideration has been selected, the static pressure in the jet can be obtained from

$$p_j = P_T - PHR.\left(P_T - p_d\right). \quad (13)$$

This allows the calculation of the jet air density from (3), and the jet air velocity from (2). Finally the orifice mass flow rate can be obtained from (1) as

$$w_j = C_d.\rho_j.V_j.A_o, \quad (14)$$

so that the ratio of mass flow rates w_j / w_d can now be determined.

In addition Sutherland's formula

$$\mu = \frac{1.458 \times 10^{-6}.T_d^{3/2}}{T_d + 110.4}, \quad (15)$$

was used to set the dynamic viscosity of air in the incompressible simulation.

4.2.2 Analysis of Results

The converged CFD solution was used to provide values of the duct static pressure, duct total pressure, jet static pressure, main duct outlet mass flow rate and jet mass flow rate. In addition the main duct static temperature and inlet M_d were known from the model boundary conditions.

A difficulty arises because the CFD simulation was carried out for incompressible flow. Under such conditions any values generated for pressures are only relative to other parts of the simulation, and so need to be adjusted to reflect the absolute pressure level. As the nominal static pressure in the main duct was known to be $p_d = 2.76 \times 10^5 Pa$, then by denoting CFD solution pressures as p^{cfd} and defining an off-set pressure p_0, we can write $p_d^{cfd} + p_0 = p_d$, so that solving for p_0, the other CFD solution pressures can be corrected to the absolute values, $P_T = P_T^{cfd} + p_0$, and $p_j = p_j^{cfd} + p_0$.

A further detail that must be included is that the simulation mass flows must be doubled before comparison with the results, this is because only one-half of the duct was modelled to take advantage of the symmetry plane down the centre of the rig.

Thereafter proceed following [1], using (4) and (10) to calculate P_T and T_T, hence obtaining $\rho_d = p_d / RT_d$, and $V_d = w_d / (A_d . \rho_d)$.

For the orifice jet, using (2) and (3) to calculate V_j and ρ_j, so that C_d is obtained from (1). The value of PHR obtained from the simulation can also be compared with the data point selected from [1].

4.3 Solution Strategy

The simulations were carried out with a fixed velocity inlet boundary condition and a mass flow split ratio for the two outlets. The fixed velocity inlet boundary condition determines the M_d of the flow in the main duct, while the mass-flow split outlet boundary conditions determine the mass flow through the orifice. FLUENT then calculates the air pressures and these, combined with the ideal jet velocity in the orifice allow the resulting pressure-head ratio and C_d to be determined.

Thus the main duct static and total pressures, together with the jet static pressure and mass flow rates are used to calculate a model C_d and PHR which were then compared with data from [1].

4.4 Details of Model

FLUENT/UNS [6] is a commercially available unstructured mesh CFD code. It uses the finite volume method of discretisation over a non-staggered grid, with interpolation carried out by a first-order, second-order or power-law scheme. The discretised equations are solved by the SIMPLE algorithm using an iterative point-based Gauss-Seidel solver with multigrid acceleration.

The cross-flow geometry was modelled in 3d in FLUENT, using incompressible flow. The geometry was meshed using a tetrahedral mesh of between ~21,000 and ~120,000 cells; prismatic cells were used for boundary layer meshing in the main duct. Only half the duct was simulated, taking advantage of the symmetry plane down the centre of the duct and through the centre-line of the orifice and jet collection duct. Use of the symmetry plane means that the solutions generated by the model have symmetrical flow patterns about that plane. The standard k-ε turbulence model was used as Re=26,200-93,600 for the present cases.

At the inlet a fixed uniform velocity profile was used as the boundary condition, allowing M_d in the main duct to be set to a predetermined value. The inlet turbulence intensity was set to 10% with a length-scale of the diameter of the duct. (Rohde et al [1] showed that the state of development of the inlet boundary layer had no appreciable influence on the discharge coefficient by comparing measurements with an entrance length of two diameters with those using an entrance length of 14 diameters.) The outlet boundary conditions were of the mass-flow-split type, that is to say a fixed proportion of the total outlet flow was constrained to flow out of each of the main duct and jet outlets.

5. EVALUATION

The cross-flow simulations covered the range of conditions indicated in Figure 4.1. These include the effect of first and second-order discretisation schemes, a mesh sensitivity study, and comparison with data for sensitivity studies against PHR and duct inlet M_d. The models are each discussed in turn in the following sections, with the key results summarised in Tables 5.1 and 5.2.

The accuracy of a simulation can be assessed by two different methods.

1. In the first the ability of the code to reproduce only the *relationship* between PHR and C_d at a given M_d is considered. In this case a model is run to convergence and

simulation data is extracted to form a PHR and C_d at a given M_d. The data [1] are then used to determine a measurement of C_d for the value of PHR obtained by the simulation. The discrepancy between the model and measured values is then expressed as the difference between the simulated and measured C_d at the resulting model PHR. (Table 5.1)

2. For the second method, mass flow split boundary conditions were selected to give a specified PHR and C_d at a specified main duct mach number, M_d, the pre-specified values of PHR and C_d being referred to as *'target'* values. If the simulation fails to accurately reproduce the relationship between the mass-flow split, M_d, pressures and C_d, then the model will not produce a PHR around the orifice which is consistent with the mass-flow split and inlet boundary conditions. In this case the discrepancy can be represented as the difference between the simulated and target values. This can be seen clearly in the incompressible simulation at high M_d (section 5.4.2), where the high air speeds in the vicinity of the orifice (a Mach number 0.8 in the orifice) caused an inaccurate calculation of pressure fields. This resulted in a simulated PHR significantly different from the target value. (Table 5.2)

The first method of evaluating the simulation accuracy is a judgement on the ability of the code to reproduce the flow physics in the vicinity of the orifice, while the second can be interpreted as a comment on the more practical difficulties involved in using mass-flow split boundary conditions to simulate cross-flow orifice cases.

5.1 Base Model

The base model evaluation was carried out using a mesh of 114,523 cells, at a PHR of 3.0 and a C_d of 0.4 with a M_d of 0.07. Simulations were carried out using both first and second order discretisation schemes.

Case		Discrepancy between FLUENT and Estimated C_d
Base Case Targets: $PHR = 3.0$ $C_d = 0.4$ $M_d = 0.07$ 114,523 cells	1st Order Achieved: $PHR = 2.984$ $C_d = 0.399$, $y^+ = 1-33$	+0.15%
	2nd Order Achieved: $PHR = 3.001$ $C_d = 0.397$, $y^+ = 1-35$	-0.25%
PHR Sensitivity $PHR = 2.0$ $C_d = 0.3$ $M_d = 0.07$ 114,523 cells	1st Order Achieved : $PHR = 2.024$ $C_d = 0.296$, $y^+ = 1-33$	-2.0%
	2nd Order Achieved : $PHR = 2.022$ $C_d = 0.296$, $y^+ = 1-33$	-2.0%
Mesh Sensitivity 1st Order $M_d = 0.07$ 21,675 cells	Target $PHR = 3.0$ Achieved : $PHR = 3.090$ $C_d = 0.390$, $y^+ = 2-212$	-3.9%
	Target $PHR = 2.0$ Achieved : $PHR = 2.050$ $C_d = 0.292$, $y^+ = 1-191$	-4.3%
Mach Number Sensitivity $PHR = 10.0$ $C_d = 0.58$ $M_d = 0.07$	1st Order 117,979 cells Achieved : $PHR = 9.508$ $C_d = 0.590$	+1.2%
	2nd Order 120,049 cells Achieved : $PHR = 9.679$ $C_d = 0.585$, $y^+_{max} = 57$	<0.17%
Mach Number Sensitivity $PHR = 10.0$ $C_d = 0.65$ $M_d = 0.25$ 141,755 cells	1st Order Achieved : $PHR = 7.756$ $C_d = 0.674$, $y^+_{max} = 117$	+8.9%
	2nd Order Achieved : $PHR = 7.882$ $C_d = 0.671$, $y^+_{max} = 135$	+8.1%

Table 5.1: Summary of Incompressible Cross-Flow Validation Results. Discrepancy in the FLUENT results with respect to the estimated C_d at the equivalent PHR values [1]. These results indicate the ability of the code to reproduce the fluid physics in the vicinity of the orifice.

Case		Discrepancy between FLUENT and Target Values	
		PHR	C_d
Base Case $PHR = 3.0$ $C_d = 0.4$ $M_d = 0.07$ 114,523 cells	1st Order	-0.5%	-0.3%
	2nd Order	+0.03%	-0.8%
PHR Sensitivity $PHR = 2.0$ $C_d = 0.3$ $M_d = 0.07$ 114,523 cells	1st Order	+1.2%	-1.3%
	2nd Order	+1.1%	-1.3%
Mesh Sensitivity 1st Order $M_d = 0.07$ 21,675 cells	$PHR = 3.0$ $C_d = 0.4$	+3.0%	-2.5%
	$PHR = 2.0$ $C_d = 0.3$	+2.5%	-2.7%
Mach Number Sensitivity $PHR = 10.0$ $C_d = 0.58$ $M_d = 0.07$	1st Order 117,979 cells	-4.9%	+1.7%
	2nd Order 120,049 cells	-3.2%	+0.86%
Mach Number Sensitivity $PHR = 10.0$ $C_d = 0.65$ $M_d = 0.25$ 141,755 cells	1st Order	-22.4%	+3.7%
	2nd Order	-21.2%	+3.2%

Table 5.2: Summary of Incompressible Cross-Flow Validation Results. The signs indicate the direction of the discrepancy in the FLUENT results with respect to the target data values [1]. These results indicate the level of agreement that might be expected for an actual test case compared with the anticipated *PHR* and C_d.

The flow was modelled incompressibly, with constant ρ=3.174kg.m^{-3}, μ=1.860kg.m^{-1}.s^{-1} and a duct static temperature of 303K. The duct inlet velocity was set to 24.4m.s^{-1} ($M_d = 0.07$) with mass-flow split boundary conditions set so that 81.7% of the inlet flow exited from the main duct outlet and 18.3% exited from the orifice collection duct outlet.

A sample of the mesh is illustrated in Figure 5.1. A close-up of the mesh around the orifice in the symmetry plane is shown in Figure 5.1(a), while 5.1(b) shows the duct cross-section at the inlet, revealing the boundary-layer mesh used along the main duct to encourage suitable development of the main duct flow profile as it approached the orifice. The main duct boundary-layer meshing was stopped half an orifice diameter before the orifice centre-line and resumed half an orifice diameter after the orifice centre-line, so that there was no boundary-layer mesh in the vicinity of the orifice itself. This was to keep the discontinuity in the mesh away from the orifice and prevented the possibility of the boundary-layer mesh from influencing flow in the vicinity of the orifice. The edges of the region where boundary-layer meshing was used appear as straight vertical lines in Figure 5.1(a). No boundary-layer meshing was used in the orifice collection duct as the flow profile was of little concern in this region, because the Rohde et al [1] data used a static pressure taken immediately down-stream of the orifice, rather than at any distance along the collection duct.

5.1.1 First-Order Discretisation

The first-order discretised simulation converged to a solution with $P_T = 279.8Pa$, $p_d = 768.3Pa$ and $p_j = -1599.5Pa$ (relative pressure values), y^+ was in the range 1-33. The outlet flows converged to the desired mass-flow splits of 81.7% and 18.3%.

The resulting solution gave $PHR = 2.984$ and $C_d = 0.399$, a discrepancy in C_d of 0.15% from an estimated value of $C_d = 0.398$ at $PHR = 2.984$. The estimated value [1] for C_d at $PHR = 2.984$ was obtained by linear interpolation using the data in Table 3.2. The results are presented in Tables 5.1 and 5.2.

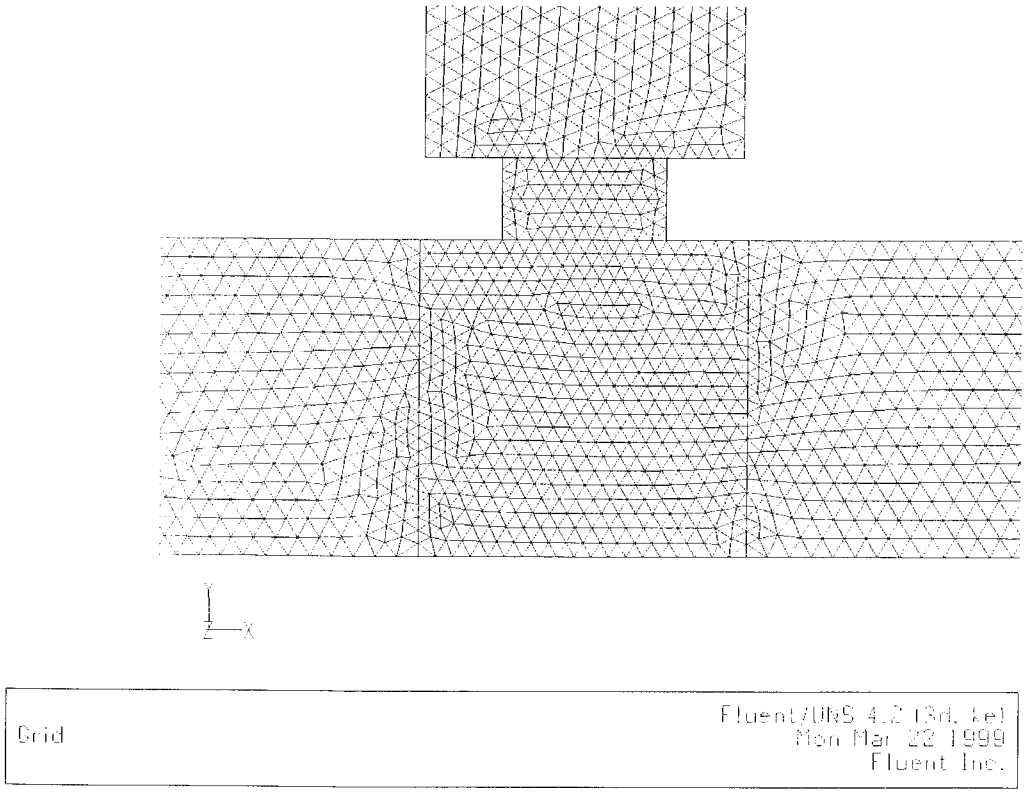

Figure 5.1(a): Symmetry plane mesh in the vicinity of the orifice.

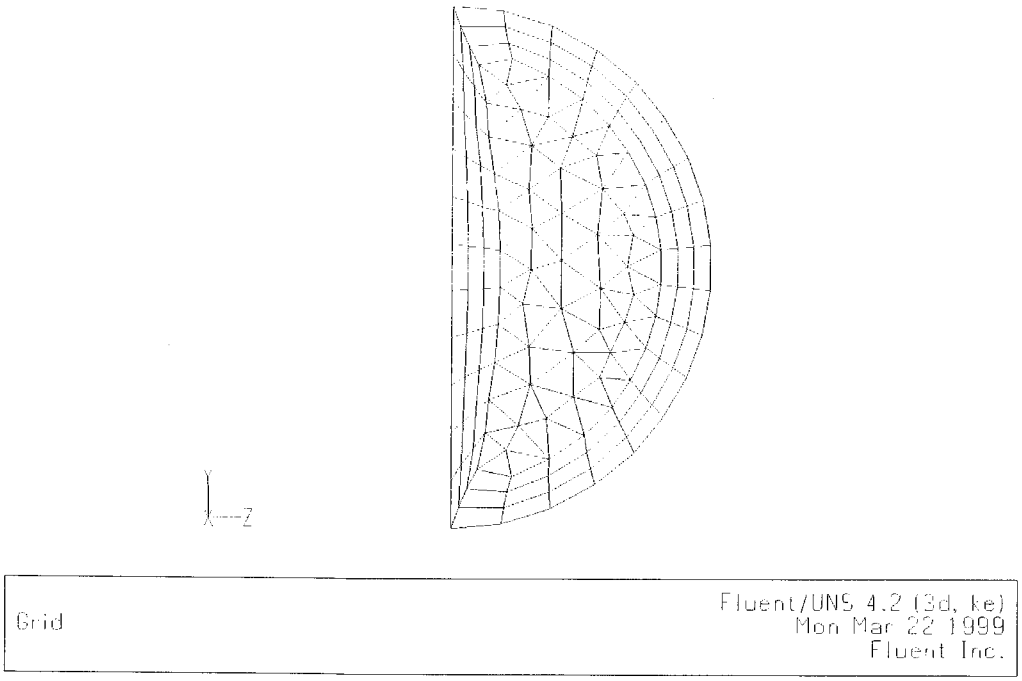

Figure 5.1(b): Inlet plane mesh showing boundary-layer meshing at edges (prisms) and interior mesh (tetrahedral).

5.1.2 Second-Order Discretisation

The converged first-order solution of section 5.1.1 was used to initialise a second-order simulation. The results are given in Tables 5.1 and 5.2. Results are shown in Figure 5.2(a)-(c); (a) shows streaklines in the vicinity of the orifice, (b) shows velocity vectors and (c) contours of static pressure in the symmetry plane around the orifice.

In both cases the discrepancies between the simulation and the data [1] are so small, that no increase in accuracy is obtained from the second-order solution.

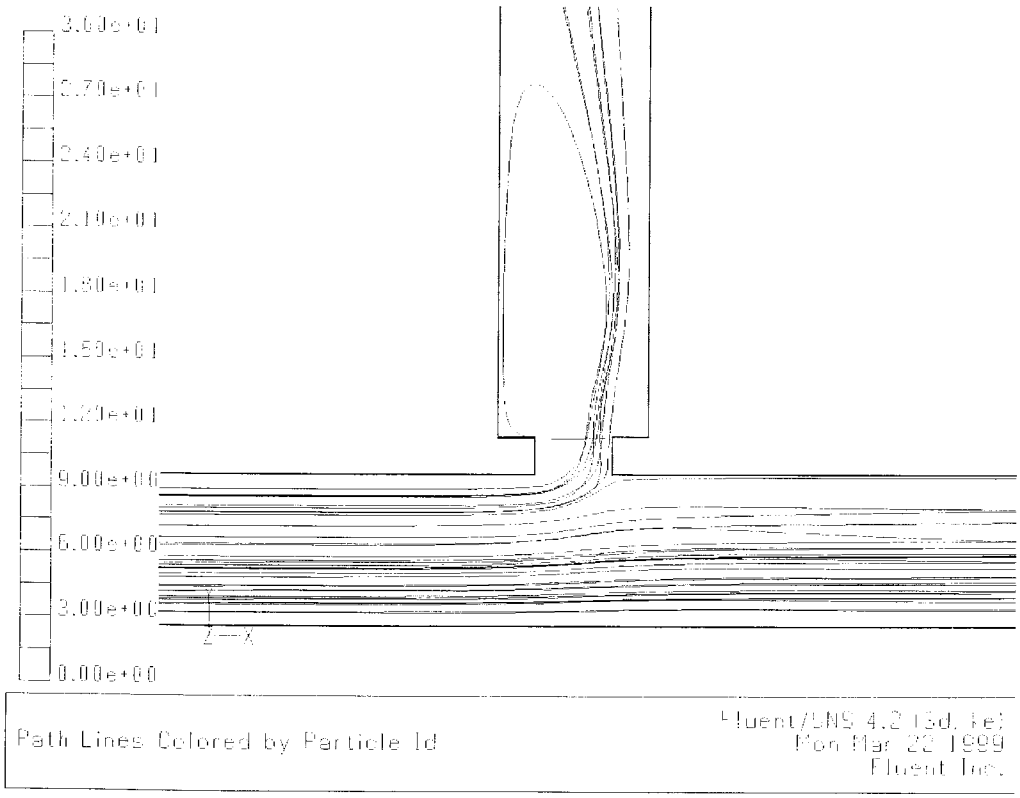

Figure 5.2(a): Particle trajectories in the vicinity of the orifice.

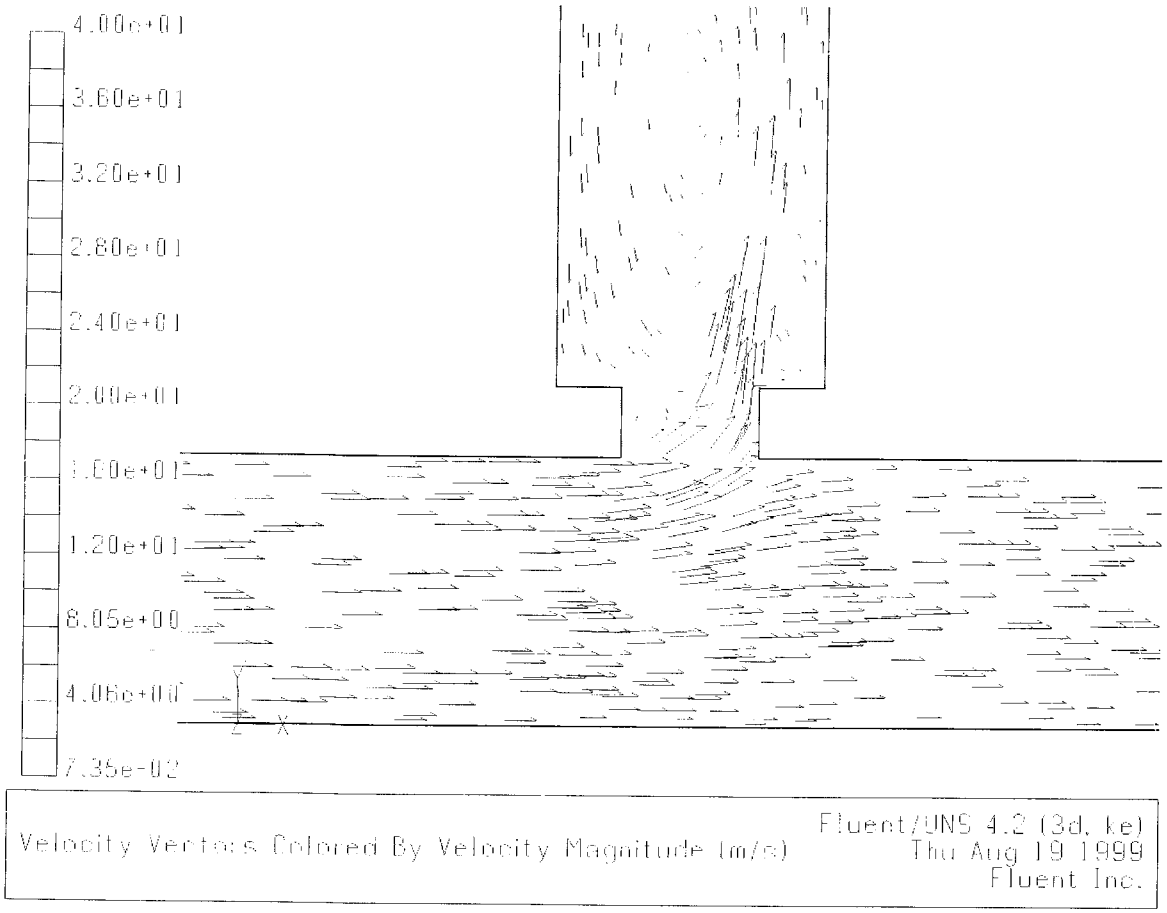

Figure 5.2(b): Velocity vectors in the vicinity of the orifice.

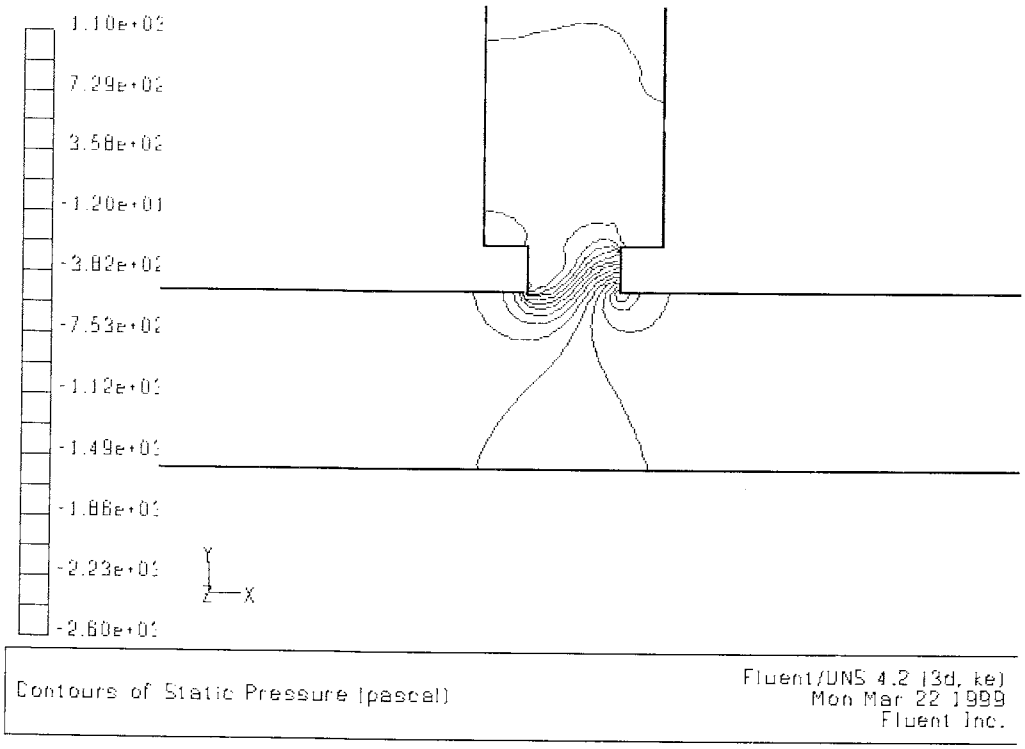

Figure 5.2(c): Contours of static pressure in the symmetry plane around the orifice.

5.2 Pressure-Head Ratio Sensitivity Study

To test whether FLUENT is able to reproduce the trend in C_d with PHR, the simulation of section 5.1 was executed under conditions for $PHR = 2.0$ and $C_d = 0.3$ with a M_d of 0.07. Simulations were carried out using both first and second order discretisation schemes.

The flow was modelled incompressibly, with constant ρ=3.174kg.m^{-3}, μ=1.860kg.m^{-1}.s^{-1} and a duct static temperature of 303K. The duct inlet velocity was set to 24.4m.s^{-1} ($M_d = 0.07$) with mass-flow split boundary conditions set so that 88.8% of the inlet flow exited from the main duct outlet and 11.2% exited from the orifice collection duct outlet.

5.2.1 Results

The results of first and second-order discretisation scheme converged solutions are given in Tables 5.1 and 5.2. Again no improvement in model accuracy was seen in the second-order solution compared with first-order discretisation.

5.3 Mesh Sensitivity Study

Simulations were carried out on a mesh of 21,675 cells at a duct inlet M_d of 0.07, thus the inlet velocity boundary condition was set to 24.4m.s^{-1}. Only first-order discretisation scheme models were run, as on such a coarse mesh, the second-order discretisation scheme had difficulty achieving convergence. Two different pressure-head ratios were covered, $PHR = 3.0$ and 2.0, the results are reported below.

5.3.1 Results

To achieve a PHR of 3.0 (i.e. a target $C_d = 0.4$), a mass-flow outlet boundary condition split of 81.7% from the main duct and 18.3% from the orifice duct was applied. For

$PHR = 2.0$ (i.e. a target $C_d = 0.3$), the mass-flow outlet boundary condition split was 88.8% from the main duct and 11.2% from the orifice duct. The resulting solution values are given in Tables 5.1 and 5.2.

5.4 Mach Number Sensitivity Study

To see whether FLUENT was able to reproduce the effect of different Mach numbers on the flow, at $PHR = 10.0$ simulations were executed with main duct inlet Mach numbers of 0.07 and 0.25. At $M_d = 0.07$ Rohde et al [1] found $C_d = 0.58$, with $C_d = 0.65$ at $M_d = 0.25$. Simulations were carried out using both first and second order discretisation schemes.

The flow was modelled incompressibly, with constant ρ=3.174kg.m^{-3}, μ=1.860kg.m^{-1}.s^{-1} and a duct static temperature of 303K.

5.4.1 Mach Number of 0.07

To simulate a main duct M_d of 0.07, the main duct velocity inlet boundary condition was set to 24.4m.s^{-1}, with mass-flow split outlet boundary conditions of 52.2% from the main duct and 47.8% from the orifice duct to achieve the desired C_d (=0.58).

First-Order Discretisation

The first-order discretisation scheme converged solution gave $PHR = 9.508$ and $C_d = 0.590$, a discrepancy in C_d of 1.2% from an estimated value [1] of $C_d = 0.583$ at $PHR = 9.508$. A mesh of 117,979 cells was used following conformal adaption on velocity gradients. (Conformal adaption is a method of mesh refinement, which leaves no hanging-nodes in the grid and smoothes out excessive mesh density gradients into the surrounding mesh. In FLUENT it is only possible to use conformal adaption with triangular or tetrahedral meshes.)

Second-Order Discretisation

The second-order discretisation scheme converged solution gave $PHR = 9.679$ and $C_d = 0.585$, a discrepancy in C_d of less than 0.17% from an estimated value [1] of $C_d = 0.585$ at $PHR = 9.679$. A mesh of 120,049 cells was used following conformal adaption on velocity gradients.

5.4.2 Mach Number of 0.25

To simulate a main duct M_d of 0.25, the main duct velocity inlet boundary condition was set to 87.2m.s^{-1}, with mass-flow-split outlet boundary conditions of 58.8% from the main duct and 41.2% from the orifice duct. For incompressible flow this would give a target $PHR = 10$ and target $C_d = 0.65$.

First-Order Discretisation

The first-order discretisation scheme converged solution gave $PHR = 7.756$ and $C_d = 0.674$, discrepancies of 22.4% and 3.7% from the target data values [1] respectively, or a discrepancy in C_d of 8.9% from an estimated value [1] of $C_d = 0.619$ at $PHR = 7.756$. A mesh of 141,755 cells was used following conformal adaption on velocity gradients. The wall-function maximum y^+ value was 117.

Conformal adaption on velocity gradients and pressure gradients was carried out using converged solutions for a range of mesh densities with between 114,523 and 141,755 cells. These showed a very gradual improvement in the solution compared with the measured data [1]. The results are shown in Figure 5.3, where the simulation value of PHR normalised by the target PHR value is shown plotted against the number of cells used in the simulation. A similar 'normalised C_d' is also plotted. The results show that a very gradual improvement in agreement between the simulated and Rohde et al [1] values of PHR and C_d takes place as the mesh is refined. This process of refinement was not continued further as the process of improvement was extremely gradual, and it seemed

likely that a significant proportion of the discrepancy would arise because an incompressible flow solution was used at $M_d = 0.25$.

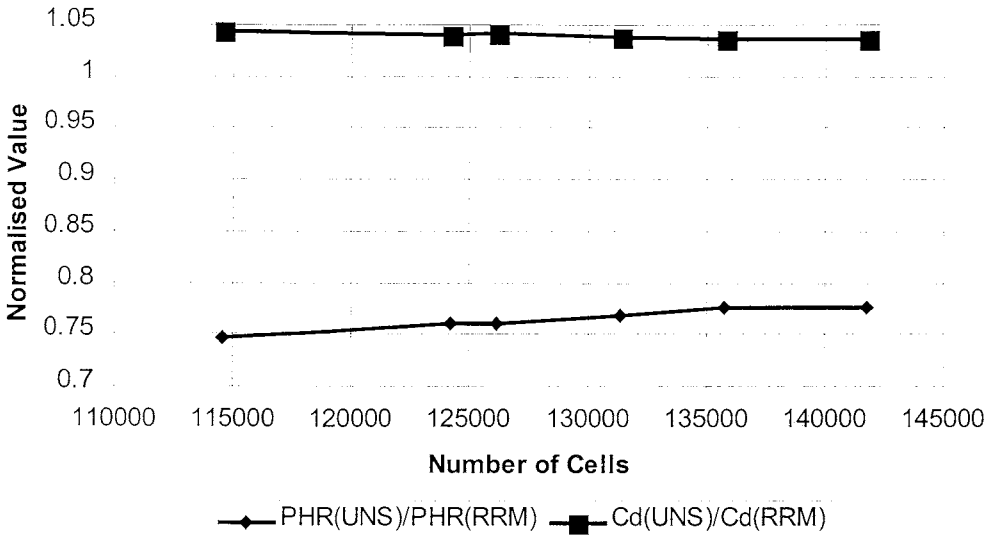

Figure 5.3: Effect of Mesh Refinement on PHR and C_d at $M_d = 0.25$. Normalised values of PHR and C_d are presented, i.e. PHR (CFD Solution)/target PHR and C_d (CFD solution)/target C_d. A normalised value of unity would indicate complete agreement between the CFD solution and the target data values [1]. The abbreviation RRM refers to Rohde et al [1].

Second-Order Discretisation

The second-order discretisation scheme converged solution gave $PHR = 7.882$ and $C_d = 0.671$, discrepancies of 21.2% and 3.2% from the target data values [1] respectively, or a discrepancy in C_d of 8.1% from an estimated value [1] of $C_d = 0.621$ at $PHR = 7.882$. A mesh of 141,755 cells was used following conformal adaption on velocity gradients. The wall-function maximum y^+ value was 135.

5.5 Comparison with Experiment

A summary of the level of agreement between the simulation results and the rig data correlation [1] is given in Tables 5.1 and 5.2. The comparisons are shown graphically in Figure 5.4. It can be seen that for $M_d = 0.07$ there is excellent agreement, with C_d predicted to better than 4.5%.

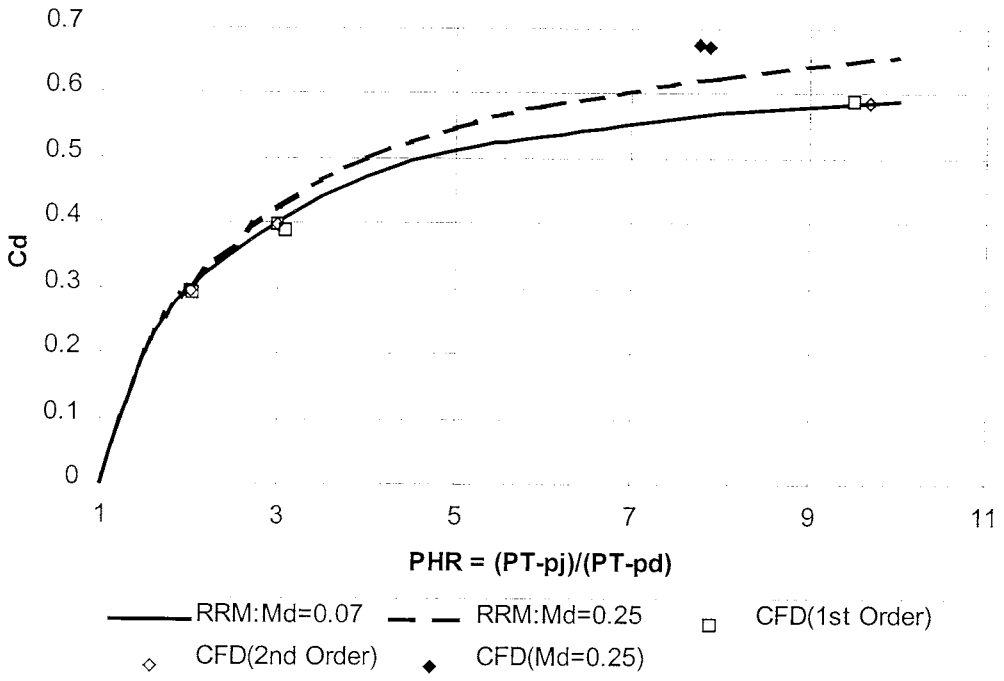

Figure 5.4: Plot of CFD simulation C_d vs. PHR (points) compared with [1] rig correlations at $M_d = 0.07$ and 0.25 (lines). In all cases except the $M_d = 0.25$ (solid points) there is excellent agreement. When $M_d = 0.25$, the orifice Mach number reached around 0.8. The abbreviation RRM refers to Rohde et al [1].

At $M_d = 0.25$ the results show less good agreement, with C_d predicted to better than 4%, but PHRs were as much as 23% low compared with the target data values. Further examination of the (incompressible) CFD simulation results showed that maximum Mach number in the converged solution (which occurred in the vicinity of the orifice) was 0.8 at a duct Mach number, $M_d = 0.25$. Under these conditions it is unsurprising that the simulation has incorrectly calculated the pressure drop across the orifice ($P_T - p_j$). As this term appears in the PHR this would explain why the CFD model solution produced an inaccurate value.

5.6 Quality Assessment

The main quality issues have been covered in other sections as the need arose, for example a mesh sensitivity study is presented in section 5.3 and sensitivity studies against PHR and main duct Mach number in sections 5.2 and 5.4. A number of other quality

issues are discussed below relating to a comparison of the data with engine conditions, the quality of the rig data [1] and the role of wall-functions in the simulation.

5.6.1 Validation as a Test Against Engine Conditions

The rig data covers orifice thickness-to-diameter aspect ratios in the range $t/d = 0.51$ to 2.83 and PHR in the range ~1.1 to 60 [1]. While the range of PHR covered is reasonable for engine conditions, engine orifice aspect ratios tend to be a little smaller than those covered by [1]. This can be seen in Figure 2.2. For this reason the validation exercise was carried out only using data from [1] with the smallest aspect ratio, $t/d = 0.51$. It is hoped that any modelling discrepancies between these and engine aspect ratios (~0.2 to 0.4) would not be significant, because for all the orifice aspect ratios considered the flow separates from the inlet lip of the orifices and then does not reattach on the upstream (with respect to the main duct flow) side of the orifice before exiting from the orifice (see e.g. Figure 5.2b).

5.6.2 Quality of Test Data

The correlations provided by [1] include a determination of the uncertainty in the rig orifice diameters (±0.0013 cm), but do not include an assessment of other experimental uncertainties in their measurements. This makes a quantitative comparison with the rig data more difficult, especially as correlation values had to be read from a graphical presentation of the results. However by taking care in extracting data from the correlation graphs, and by only requiring agreement between simulation and data to 5%, it would seem unlikely that such difficulties would affect the results of the validation to any significant degree.

5.6.3 Wall-Function y^+

The results showed excellent agreement with the [1] data, despite having wall-function y^+ values outside the recommended ranges. This implies that the flow pattern, PHR and C_d

are not sensitive to the value of y^+ obtained, and that the flow is not sensitive to boundary-layer conditions.

6. DISCUSSION

Generally a high level of agreement was achieved between the FLUENT simulations and the Rohde et al data [1], with discrepancies between the predicted values and data less than 5% for PHR and C_d.

For the case with a main duct Mach number, $M_d = 0.25$, agreement was less good, with a discrepancy of 21% in PHR with [1]. This can be accounted for by considering the Mach number in the vicinity of the orifice, which was much higher (0.8) than that in the main duct. Under these conditions it is to be expected that an incompressible simulation will fail to correctly predict the orifice pressure-drop, resulting in an incorrect value of PHR.

At lower Mach numbers, with $M_d = 0.07$, and the orifice Mach number around 0.2 the simulations reproduced the trend in the Rohde et al correlations [1] with PHR (see Figure 5.4).

The mesh sensitivity studies were carried out with a grid of 21,675 cells. Despite the coarseness of the mesh, excellent agreement to 3% or better in both PHR and C_d was obtained. The range of y^+ values covered in the simulations implies that the solutions were insensitive to boundary-layer modelling, suggesting that boundary-layer flows are not important in the fluid dynamics of the cross-flow problem under these conditions.

7. LESSONS LEARNED

- Despite having a main duct Mach number of 0.25, if the Mach number in the vicinity of the orifice is too high (in this case 0.8 in the orifice), incompressible flow modelling will give inaccurate predictions of the orifice pressure-drop. Such cases should be

simulated using a compressible flow model. No similar difficulties were encountered with main duct Mach numbers of 0.07, giving orifice Mach numbers of around 0.2.

- Accurate solutions (better than 5% in both PHR and C_d) were predicted despite using a coarse mesh (~22,000 cells) and having wall-function y^+ values outside the recommended range of 12-100. This implies that boundary-layer effects are unimportant in determining the flow.

8. CONCLUSIONS

1. Validation of FLUENT/UNS version 4.2 using incompressible flow modelling has been carried out against cross-flow data from Rohde et al [1] for pressure-head ratios in the range 2-10 and main duct Mach numbers of 0.07 and 0.25.
2. At main duct Mach numbers of 0.07, excellent agreement was obtained between CFD and rig data, with predicted differences in pressure-head ratios and discharge coefficients less than 5% in all the cases covered.
3. The CFD simulation correctly reproduced the trend in discharge coefficients with pressure-head ratio at a main duct Mach number of 0.07, over a range of pressure-head ratios of between 2 and 10.
4. Mesh sensitivity studies for the case with a main duct Mach number of 0.07, and for pressure-head ratios of 2 and 3, showed excellent agreement with rig data (better than 5% in pressure-head ratio and discharge coefficient), indicating that the solutions were close to mesh convergence.
5. For main duct Mach numbers of 0.25 agreement with rig data was less good because the Mach number in the vicinity of the orifice was 0.8. This confirmed the expectation that under these conditions incompressible flow modelling would not be adequate, so differences between rig and predicted pressure-head ratios of around 20% were unsurprising.
6. Engine orifices at Rolls-Royce have aspect ratios in the range 0.2-0.4 and engine pressure-head ratios of around 1-60. These compare with the validation orifice aspect ratio of 0.51 (the smallest given by Rohde et al [1]) and pressure-head ratios in the range 2-10.

9. ACKNOWLEDGEMENT

The author gratefully acknowledges help and advice from Dr Nick Hills of the University of Sussex.

10. REFERENCES

1. Rohde, J E, Richards, H T and Metger, G W (1969), Discharge coefficients for thick plate orifices with approach flow perpendicular and inclined to the orifice axis, NASA Technical Note, NASA TN D-5467, 29 pages.
2. Rayer, Q G and Snowsill, G D (1998), Validation of FLUENT against incompressible and compressible flow through orifices, IMechE, CFD in Fluid Machinery Design, ISBN 1-86058-165-X, ISSN 1357-9193, S546/010/98, pp. 79-91.
3. Rayer, Q G and Snowsill, G D (1999), FLUENT validation for incompressible flow through a 0.5 aspect ratio orifice and compressible flow through a sharp-edged slit, NAFEMS Int J CFD Case Studies, Vol 2, *in the press May 1999.*
4. Rayer, Q G (1999), Computational fluid dynamics guidelines for best working practice, *submitted to NAFEMS Int J CFD Case Studies, April 1999.*
5. Hay, N and Lampard, D (1996), Discharge coefficient of turbine cooling holes: a review, Trans ASME, 96-GT-492.
6. FLUENT (1996), User's guide for FLUENT/UNS and RAMPANT, release 4.0, April 1996, Fluent Incorporated, Centerra Resource Park, 10 Cavendish Court, Lebanon, NH 03766, USA.
7. Versteeg, H K and Malalasekera, W (1995), An introduction to computational fluid dynamics, Longman Group Ltd., ISBN 0-582-21884-5, 257 pages.